MIT Libraries | DSpace@MIT

MIT Open Access Articles

NICER detection of strong photospheric expansion during a thermonuclear x-ray burst from 4U 1820-30

Massachusetts Institute of Technology

NICER Detection of Strong Photospheric Expansion during a Thermonuclear X-Ray Burst from 4U 1820–30

L. Keek[1], Z. Arzoumanian[2], D. Chakrabarty[3] , J. Chenevez[4] , K. C. Gendreau[2], S. Guillot[5,6], T. Güver[7,8] , J. Homan[9,10] ,
G. K. Jaisawal[4] , B. LaMarr[3], F. K. Lamb[11,12], S. Mahmoodifar[2] , C. B. Markwardt[2] , T. Okajima[2], T. E. Strohmayer[2], and
J. J. M. in 't Zand[10]

[1] Department of Astronomy, University of Maryland, College Park, MD 20742, USA; lkeek@umd.edu
[2] X-ray Astrophysics Laboratory, Astrophysics Science Division, NASA/GSFC, Greenbelt, MD 20771, USA
[3] MIT Kavli Institute for Astrophysics and Space Research, Massachusetts Institute of Technology, Cambridge, MA 02139, USA
[4] National Space Institute, Technical University of Denmark, Elektrovej 327-328, DK-2800 Lyngby, Denmark
[5] CNRS, IRAP, 9 avenue du Colonel Roche, BP 44346, F-31028 Toulouse Cedex 4, France
[6] Université de Toulouse, CNES, UPS-OMP, F-31028 Toulouse, France
[7] Department of Astronomy and Space Sciences, Science Faculty, Istanbul University, Beyazıt, 34119 Istanbul, Turkey
[8] Istanbul University Observatory Research and Application Center, Beyazıt, 34119 Istanbul, Turkey
[9] Eureka Scientific, Inc., 2452 Delmer Street, Oakland, CA 94602, USA
[10] SRON, Netherlands Institute for Space Research, Sorbonnelaan 2, 3584 CA Utrecht, The Netherlands
[11] Center for Theoretical Astrophysics and Department of Physics, University of Illinois at Urbana-Champaign, Urbana, IL 61801, USA
[12] Department of Astronomy, University of Illinois at Urbana-Champaign, Urbana, IL 61801, USA

Abstract

The *Neutron Star Interior Composition Explorer* (*NICER*) on the International Space Station (ISS) observed strong photospheric expansion of the neutron star in 4U 1820–30 during a Type I X-ray burst. A thermonuclear helium flash in the star's envelope powered a burst that reached the Eddington limit. Radiation pressure pushed the photosphere out to ∼200 km, while the blackbody temperature dropped to 0.45 keV. Previous observations of similar bursts were performed with instruments that are sensitive only above 3 keV, and the burst signal was weak at low temperatures. *NICER*'s 0.2–12 keV passband enables the first complete detailed observation of strong expansion bursts. The strong expansion lasted only 0.6 s, and was followed by moderate expansion with a 20 km apparent radius, before the photosphere finally settled back down at 3 s after the burst onset. In addition to thermal emission from the neutron star, the *NICER* spectra reveal a second component that is well fit by optically thick Comptonization. During the strong expansion, this component is six times brighter than prior to the burst, and it accounts for 71% of the flux. In the moderate expansion phase, the Comptonization flux drops, while the thermal component brightens, and the total flux remains constant at the Eddington limit. We speculate that the thermal emission is reprocessed in the accretion environment to form the Comptonization component, and that changes in the covering fraction of the star explain the evolution of the relative contributions to the total flux.

Key words: accretion, accretion disks – stars: individual (4U 1820–30) – stars: neutron – X-rays: binaries – X-rays: bursts

1. Introduction

Located in the globular cluster NGC 6624, 4U 1820–30 is an ultracompact X-ray binary with an orbital period of 11.4 minutes (Stella et al. 1987). Material of predominantly helium composition is accreted onto the neutron star (e.g., Cumming 2003), where runaway thermonuclear burning powers the X-ray bursts that have been observed from this source since 1975 (Grindlay et al. 1976; for a recent review, see Galloway & Keek 2017). In the absence of hydrogen, nuclear burning proceeds rapidly, unhindered by waiting points from weak decays (e.g., Weinberg et al. 2006). Most fuel, therefore, burns at the onset, and a high peak luminosity is reached quickly. When the luminosity exceeds the Eddington limit, radiation pressure exceeds the gravitational pull, and photospheric radius expansion (PRE) is the result (Grindlay et al. 1980). During PRE, the luminosity remains near the Eddington limit. An increase in the emitting area due to expansion, therefore, is accompanied by a decrease of the photospheric temperature.

For most PRE bursts the observed blackbody radius increases by a factor of a few, whereas a small subset of PRE bursts exhibit strong expansion in excess of a factor 10 (e.g., Galloway

et al. 2008). A radius increase of a factor >100 is referred to as "superexpansion" (in 't Zand & Weinberg 2010). Strong expansion may drive a wind from the neutron star (e.g., Ebisuzaki et al. 1983; Paczynski & Proszynski 1986) and provide opportunities to constrain the neutron star's compactness (e.g., van Paradijs & Lewin 1987; in 't Zand & Weinberg 2010).

With instruments like the Proportional Counter Array (PCA; Jahoda et al. 2006) on board the *Rossi X-ray Timing Explorer* (*RXTE*) the temperature decrease during the expansion leads to a substantial loss of signal out of the 3–60 keV passband, producing a characteristic dip in the burst light curve (Paczynski 1983). For the strongest expansion, the spectral parameters could not be reliably measured. The passband of the *Neutron Star Interior Composition Explorer* (*NICER*; Gendreau & Arzoumanian 2017) on the International Space Station (ISS), however, extends down to 0.2 keV, making it an ideal instrument to study strong expansion at high time resolution. Older instrumentation with a similar passband has observed bursts with at most moderate expansion (e.g., in 't Zand et al. 2013).

In this Letter we study the first strong PRE burst from 4U 1820–30 detected with *NICER*. The instrument and

observations are introduced in Section 2. Time-resolved spectroscopy shows that *NICER* can track the thermal burst emission as well as a Comptonization component throughout the expansion phase (Section 3). For the first time we can test models of expansion and wind generation (Section 4), and we discuss the prospects for future *NICER* studies of strong radius expansion bursts (Section 5).

2. Observations

In 2017 August, 4U 1820–30 was in the hard spectral state (Section 3.1), and over 2.2 days *NICER* observed the source for a total good exposure of 60.9 ks. Five bursts were detected, each with a short duration ($\sim$5 s) and a high peak count rate ($\sim$2 $\times$ 10^4 c s^{-1}). We perform a detailed analysis of the first burst in ObsID 1050300108 on MJD 57994.37115 (2017 August 29).

The X-ray Timing Instrument (XTI; Gendreau et al. 2016) on board *NICER* employs 56 co-aligned X-ray concentrator optics and silicon-drift detectors (Prigozhin et al. 2012), with 52 in operation. This configuration enables the detection of X-ray photons in the 0.2–12 keV passband at high time resolution and <100 eV energy resolution, with a peak effective area of 1900 cm^2 at 1.5 keV. We create XTI spectra with HEASOFT version 6.22.1 and NICERDAS 2017-09-06_V002. The spectra are analyzed with XSPEC 12.9.1p (Arnaud 1996) and version 0.06 of the *NICER* response files. As background we use the blank-field spectrum of Keek et al. (2018), which is appropriate for the conditions of our observation with a low particle background and the ISS being on the night-side of the Earth. For our analysis, we group neighboring spectral bins to ensure a minimum of 15 counts per bin.

3. Results

3.1. Persistent Emission

The burst happened near the start of the *NICER* pointing. Therefore, we characterize the persistent emission using a 2145 s interval at the end of the 2294 s pointing. We extract a spectrum in the 0.3–9.0 keV band with 3.9 $\times$ 10^6 counts (see Figure 2 below). Following the broadband analysis by Costantini et al. (2012), we fit the persistent emission with a combination of a Planck model (bbodyrad in XSPEC) and a Comptonization component (compTT; Titarchuk 1994a). The Tübingen-Boulder model (TBabs) for interstellar absorption is employed with abundances from Wilms et al. (2000). The fit exhibits residuals near the instrumental edges around 0.5 keV and 2.3 keV. This indicates a small shift in the gain that is not included in the current model of the instrument response. We use XSPEC's gain model to optimize the energy scale of our data, finding a gain offset of 4.5 eV and slope of 1.008, which is small with respect to the $\sim$100 eV energy resolution. This substantially improves the fit, but some features remain in the residuals. Further improvements to the response model are needed to fully resolve these issues. In this study we regard it a systematic uncertainty. A goodness of fit per degree of freedom of $\chi^2_\nu = 1.0$ ($\nu = 860$) is obtained by adding a 1.5% error in quadrature to the statistical error of each data point.

The best-fitting parameter values and 1σ uncertainties are presented in Table 1. The absorption column, $N_{\rm H}$, is consistent within 1σ with the mean value obtained from *Chandra* grating spectra (Güver et al. 2010). We use the cflux model to determine

Table 1
Best Fit to the Persistent Spectrum

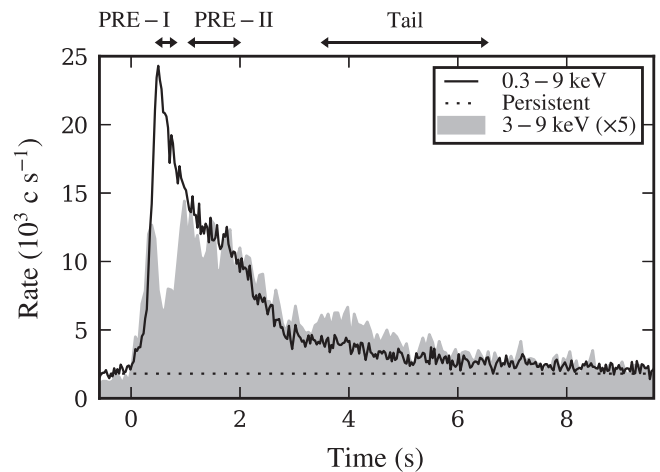| Parameter	Value
TBabs	
$N_{\rm H}(10^{21}\,{\rm cm}^{-2})$	2.53 ± 0.02
bbodyrad	
kT(keV)	0.561 ± 0.007
$R_{\rm bb}$(km at 8.4 kpc)	21.2 ± 0.5
compTT	
kT_0(keV)	0.04 ± 0.02
kT(keV)	2.69 ± 0.06
τ	7.60 ± 0.12
$K_{\rm compTT}$(c s^{-1} keV^{-1})	2.4 ± 0.9
$F_{0.3-9\,{\rm keV}}(10^{-9}\,{\rm erg\,s}^{-1}\,{\rm cm}^{-2})$	6.89 ± 0.02

Figure 1. Photon count rate as a function of time in the 0.3–9 keV passband at 30 ms resolution. The top of the shaded region marks the 3–9 keV count rate for comparison (scaled by a factor of 5). The dotted line indicates the persistent count rate measured at the end of the observation. On top, three time intervals are indicated for spectroscopy (Figure 2).

the unabsorbed Comptonization flux in the 0.3–9.0 keV band to be $(6.31 \pm 0.03) \times 10^{-9}$ erg s^{-1} cm^{-2} and by extrapolation to the 0.001–100 keV band we derive an unabsorbed bolometric flux of $(8.86 \pm 0.09) \times 10^{-9}$ erg s^{-1} cm^{-2}.

From the normalization of the blackbody we derive the apparent radius, $R_{\rm bb} = 21.2 \pm 0.5$ km, under assumption of an isotropically emitting spherical surface at a distance of 8.4 kpc (Valenti et al. 2004). This is larger than expected for the neutron star, and may represent emission from the inner disk. We caution that the best-fit blackbody parameters may be sensitive to the energy kT_0 of the seed photons being Comptonized. Including the blackbody component, the total unabsorbed persistent flux is $(6.89 \pm 0.02) \times 10^{-9}$ erg s^{-1} cm^{-2} (0.3–9.0 keV) or $(9.54 \pm 0.09) \times 10^{-9}$ erg s^{-1} cm^{-2} (0.001–100 keV).

As a measure of the Eddington flux, we find from the Multi-instrument Burst Archive (e.g., Galloway et al. 2008) the weighted mean of the bolometric peak blackbody flux of 67 PRE bursts observed with *RXTE*/PCA from 4U 1820–30: $F_{\rm Edd} = (6.08 \pm 0.06) \times 10^{-8}$ erg s^{-1} cm^{-2}. Therefore, the total persistent flux measured with *NICER* is $(0.157 \pm 0.002)F_{\rm Edd}$.
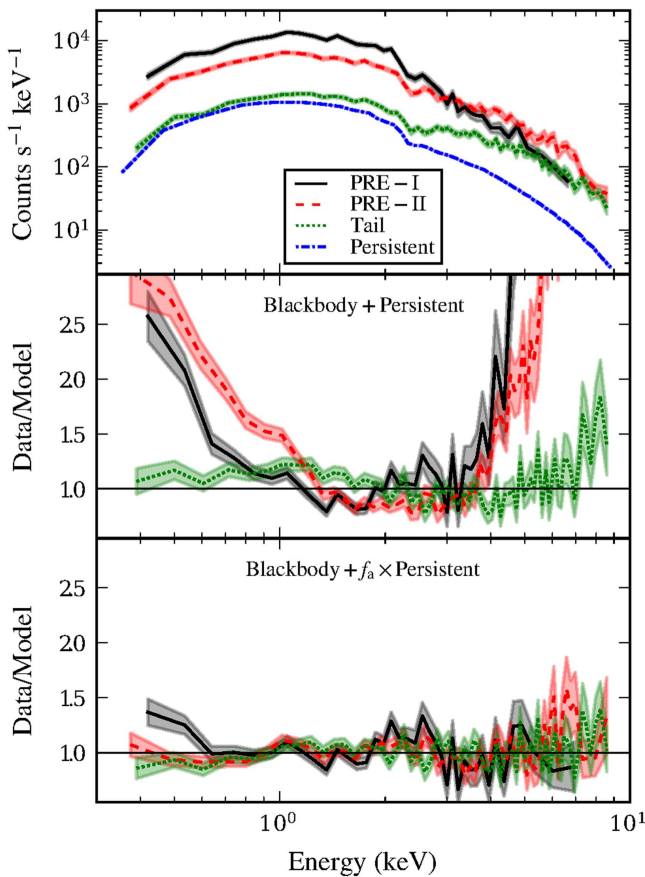
Figure 2. Top panel: X-ray spectra from three intervals in the burst (Figure 1) as well as the persistent emission. The spectra are rebinned to a resolution of at most 50 eV, and shaded bands indicate the 1σ uncertainty ranges. Middle panel: ratio of the burst spectra and best-fitting models with an absorbed blackbody and fixed persistent Comptonization component. Bottom panel: ratios for similar fits where the persistent Comptonization component is scaled with independent factors f_a.

3.2. Burst Light Curve

The burst light curve reaches a peak count rate of 2.4×10^4 c s^{-1} in the 0.3–9 keV band (Figure 1). When we consider only the photons with energies in excess of 3 keV, where past instruments such as *RXTE*/PCA were sensitive, a dip appears in the light curve. Such a dip has been found to be the characteristic signature of PRE (Grindlay et al. 1980). *NICER*'s coverage of the soft X-ray band provides a complementary view of this bright burst phase, and the count rate spikes. The XTI's modularity accommodates these large count rates without pile-up or telemetry issues. The high count rate is maintained for a short duration ($\sim$0.5 s), and is quickly reduced to $\sim 1.2 \times 10^4$ c s^{-1}. The latter level appears as a $\sim$0.5 s "plateau," after which the count rate returns to the persistent level on a timescale of $\sim$8 s.

No burst oscillations have been detected during this burst.

3.3. Burst Spectra

To investigate the importance of the different spectral components during the burst, we extract spectra from three time intervals. We select an interval of 0.33 s around the peak in the count rate ("PRE-I"; Figures 1, 2), 0.9 s in the subsequent plateau ("PRE-II"), and 3 s in the tail ("Tail"). We first fit the spectra with the usual burst model, where we keep the

Comptonization component parameters fixed at the values from Table 1 and employ the blackbody component to model the thermal burst emission. The absorption column, N_H, is fixed to the best-fitting value from the persistent emission. Furthermore, we use the same gain corrections as in Section 3.1. This spectral model does not provide a satisfactory description of the data ($\chi^2_\nu(\nu) = 2.38(236)$, $4.08(343)$, and $1.21(358)$ for PRE-I, PRE-II, and the tail, respectively), with excesses appearing at both ends of the passband (Figure 2, middle panel). Next, we allow for a scaling factor, f_a, to change the normalization of the Comptonization component (e.g., Worpel et al. 2013). This scaling is a purely phenomenological assumption. Using this scaling, the fits are vastly improved ($\chi^2_\nu(\nu) = 1.37(235)$, $1.12(342)$, and $0.94(357)$ for PRE-I, PRE-II, and the tail, respectively), and provide a reasonable description of the spectra (Figure 2, bottom panel). We employ this "f_a model" in time-resolved spectroscopy. In all of these fits, the seed and electron temperatures of the Comptonization component during the burst are fixed at the values found for the persistent emission (Table 1). Although this produces good fits, it is not a self-consistent physical model.

Instead of Comptonization, we also tested the same model for disk reflection that was successfully applied to the 1999 superburst from 4U 1820–30 (Ballantyne & Strohmayer 2004). It fails to provide an adequate fit, especially for the excess at $\gtrsim 3$ keV (Figure 2, middle panel). We find a 90% upper limit to the reflection fraction of $f_{refl} = 0.22$, which is close to the value measured in the superburst.

3.4. Time-resolved Spectroscopy

We extract spectra from 52 time intervals with durations between 0.03 s where the count rate peaks and 1.92 s in the tail. On average, the spectra contain 1239 counts each (6.4×10^4 counts in total).

The spectra are fit with the f_a model (Section 3.3). Strong photospheric expansion is apparent (Figure 3): R_{bb} reaches a maximum of $R_{bb} = 190 \pm 10$ km, accompanied by a minimum in the temperature of $kT = 0.449 \pm 0.013$ keV (weighted means of six bins around the extrema). The phase of strong expansion lasts only $\sim$0.6 s. The subsequent decrease in radius slows down, however, for $\sim$1 s during a plateau of moderate expansion with $R_{bb} = 13.5 \pm 1.3$ km and $kT = 1.7 \pm 0.2$ keV. The end of the PRE phase ("touchdown") is marked by a peak in kT around 3 s, coinciding with a brief dip in R_{bb} (see also, e.g., Zhang et al. 2013), after which R_{bb} remains stable ($R_{bb} = 6.3 \pm 0.3$ km). R_{bb} in the strong and moderate PRE phases are, respectively, 30 ± 2 and 2.1 ± 0.2 times the value in the tail. At touchdown, the temperature is near $kT \simeq 3$ keV, but the uncertainties are large. For this value of kT, the peak of the photon counts spectrum is near 6 keV, where the *NICER* effective area is substantially reduced with respect to its peak around $\sim$1.5 keV.

At the burst onset there is a strong rise in f_a to a mean value of $f_a = 5.99 \pm 0.12$. During the moderate expansion phase, f_a begins to decline, returning to unity (the persistent level) in the burst tail.

The total unabsorbed bolometric flux peaks at a plateau with a weighted mean value of $(7.52 \pm 0.12) \times 10^{-8}$ erg s^{-1} cm^{-2}, which is maintained up to touchdown (Figure 4 top). Subtracting the persistent emission, it is 8.0% larger than F_{Edd} for the *RXTE*/PCA bursts (Section 3.1). This falls within the typical observed variations in the peak fluxes of PRE bursts
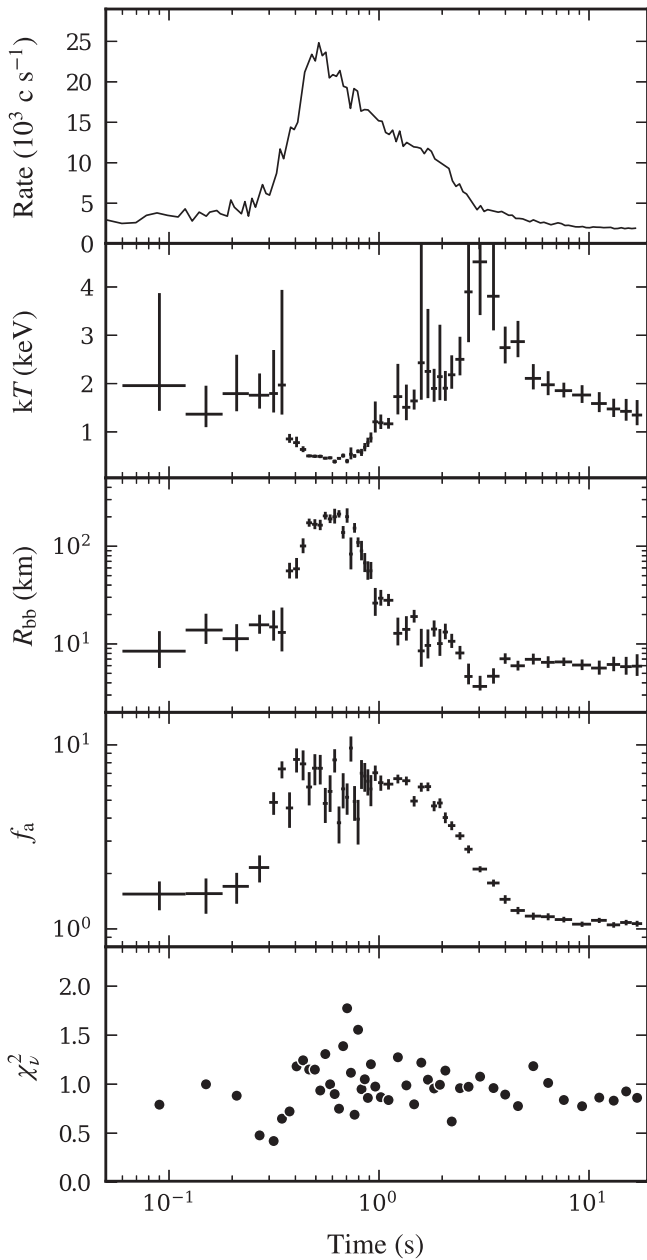
Figure 3. Results of time-resolved spectroscopy. The top panel shows the count rate, the bottom panel shows the goodness of fit χ_ν^2, and the other panels show the best-fitting values with 1σ errors for the blackbody temperature kT, radius of the emitting area R_{bb} (assuming a distance of 8.4 kpc), and scaling factor for the persistent Comptonization flux f_a.
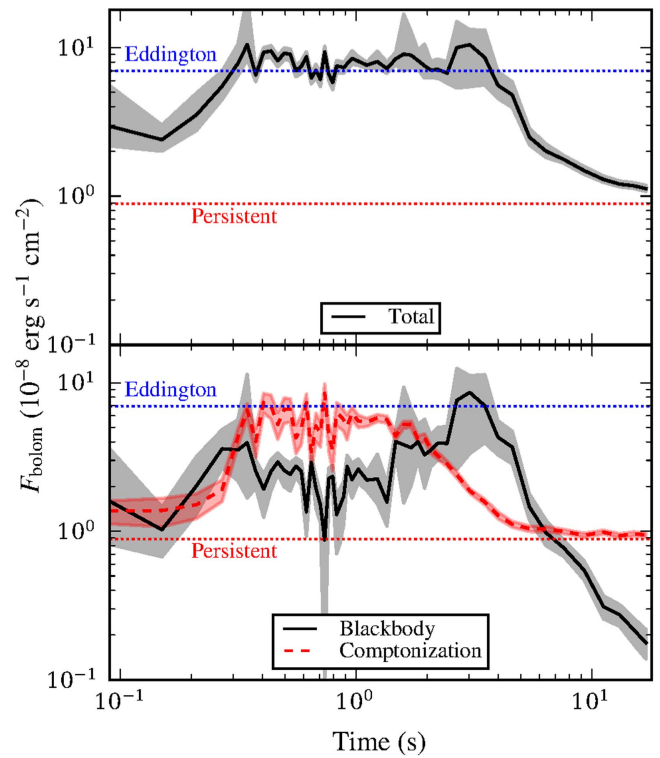

Figure 4. Unabsorbed bolometric flux as a function of time. Top panel: total flux (the shaded band indicates the 1σ uncertainty range), with horizontal dotted lines indicating the persistent flux outside of the burst and the *RXTE*/ PCA Eddington flux (*NICER* persistent flux included). Bottom panel: flux for both components separately.

of the same source (e.g., Kuulkers et al. 2003). Integrating the flux above the persistent level, we find a total burst fluence of $(4.0 \pm 1.1) \times 10^{-7}\,\mathrm{erg\,cm^{-2}}$.

When we regard the two spectral components separately, the blackbody fluence is $(2.8 \pm 1.0) \times 10^{-7}\,\mathrm{erg\,cm^{-2}}$, and the Comptonization fluence in excess of the persistent level is $(1.2 \pm 0.2) \times 10^{-7}\,\mathrm{erg\,cm^{-2}}$. Therefore, a fraction of 0.29 ± 0.10 of the total burst fluence is in the Comptonization component. Prior to $t \simeq 1.3\,\mathrm{s}$, the fraction is 0.71 ± 0.03. Subsequently, the blackbody flux increases up to the touchdown, whereas the Comptonization flux decreases. At $t = 3\,\mathrm{s}$ the flux fraction for Comptonization is 0.18 ± 0.05.

After the touchdown at $t = 3\,\mathrm{s}$, the blackbody flux drops as a power law. Following the prescription of in 't Zand et al. (2017), we fit a power law to the blackbody flux decline, and find an index $\Gamma = 2.0 \pm 0.2$, which is typical for short bursts from helium-rich fuel (in 't Zand et al. 2014, 2017). Similarly, we determine the power-law slope of the decay of the Comptonization component in the 2–4 s time interval: $\Gamma = 1.46 \pm 0.07$.

4. Discussion

4.1. Comparison to Expansion and Wind Models

The 1980s saw the first models of PRE and radiation-driven winds for the most luminous bursts (e.g., Ebisuzaki et al. 1983; Paczynski 1983). Paczynski & Proszynski (1986, p. 529) created general relativistic models that allowed them to probe strong expansion, and they remarked "Most likely, the stars with winds are too cool to be detectable with the existing X-ray instruments." With the *NICER* observations of 4U 1820–30 we finally have the soft X-ray coverage at high time resolution to test these models and investigate the strong radius expansion regime. Their model with mass outflow rate $\dot{M}_0 = 10^{17.5}\,\mathrm{g\,s^{-1}}$ predicts a photospheric radius that is within 1σ of the maximum $R_{bb} = 190 \pm 10\,\mathrm{km}$ that we derive. The predicted photospheric temperature of 0.48 keV is close to our measured minimum of $kT = 0.449 \pm 0.013\,\mathrm{keV}$.

The model predicts an outflow velocity of $\simeq 790\,\mathrm{km\,s^{-1}}$. This value is strongly dependent on the outer boundary conditions, such as the optical depth where the observed signal

originates: different conditions give velocities in the range of 700–5000 km s^{-1}. The large change in R_{bb} within 0.12 s at the burst onset suggests an expansion of $(1.5 \pm 0.4) \times 10^3$ km s^{-1}, which may be a lower limit on the outflow velocity.

In comparing our observations to these models, we included neither the systematic uncertainties from the source distance, anisotropy factors (e.g., He & Keek 2016), and color corrections of the blackbody parameters (e.g., Suleimanov et al. 2012), nor the gravitational redshift. Nevertheless, it is encouraging that the observed properties of the strong PRE phase are well described by these relatively simple models. Predictions from models with improved boundary conditions (Joss & Melia 1987) and radiation transport (Nobili et al. 1994) differ by factors of only a few.

4.2. Comparison to Previous Bursts: Superexpansion

During superexpansion bursts observed by *RXTE*/PCA, the thermal emission moved below the 3–60 keV passband, and even the persistent component disappeared (in 't Zand & Weinberg 2010). This was observed from 4U 1820–30 at a low persistent flux. During bursts at ~2–3 times higher persistent flux, the source remained detectable, even though the bursts had a similar fluence and duration. in 't Zand et al. (2012) speculated that higher accretion rates affect photospheric expansion through the ram pressure of the infalling material. The *NICER* burst occurred at a relatively high persistent flux, which corresponds to a mass accretion rate of $\dot{M} = (2.96 \pm 0.04) \times 10^{17}$ g s^{-1} (for hydrogen-deficient material and a 10 km neutron star radius). This is close to the model-predicted outflow rate $\dot{M}_0$. The ram pressure from accretion may have been important in setting the extent of the expansion, whereas superexpansion occurs only at lower accretion rates and ram pressures (in 't Zand et al. 2012). To accurately predict the expansion behavior, future models need to include the accretion flow, and compare its ram pressure to that of the outflow.

4.3. Enhanced Comptonization Emission

The Comptonization component in our phenomenological model becomes six times brighter during the burst. We discuss potential interpretations of this component and of its time evolution.

Model spectra for strongly expanded atmospheres deviate from a blackbody due to Comptonization and free–free absorption and emission (e.g., Titarchuk 1994b). Our observed Comptonization component is substantially brighter than the model predictions, and may instead be produced by reprocessing of burst emission in the accretion environment. For example, a spreading layer of accreted material could cover a substantial fraction of the stellar surface during PRE (e.g., Kajava et al. 2017), and its spectrum is thought to be well described by optically thick Comptonization emission with a temperature of $kT \simeq 2.5$ keV (Suleimanov & Poutanen 2006; Revnivtsev et al. 2013), similar to our `compTT` component (Table 1).

Alternatively, the burst emission could undergo Compton scattering in the disk or corona. In the strong PRE phase, the Comptonization component contributes 71% of the flux. For such a large fraction of the neutron star's thermal emission to be intercepted, the disk or its corona must have a large scale height close to the star (e.g., He & Keek 2016). The flux

fraction remains constant in this phase, despite large variations in R_{bb}. The fraction only decreases in the moderate PRE phase, once R_{bb} drops below ~20 km. If the optically thick disk/corona is truncated at this radius, the whole neutron star is revealed when the star's atmospheric radius becomes smaller than the disk's inner radius. A truncated disk is expected in the hard spectral state (see also the discussion in in 't Zand et al. 2012). In this scenario, part of the neutron star is covered during the strong PRE phase, and our measurement of R_{bb} represents the visible fraction of the neutron star surface. If the total flux were produced by the blackbody component, the larger normalization suggests a maximum expansion of $R_{bb} = 350 \pm 40$ km.

If the thermal emission is Comptonized, one expects the spectral shape of the Comptonization component to change with the blackbody temperature. Nevertheless, we obtain good fits with a fixed shape, despite changes in the blackbody temperature and the Compton component luminosity. This is similar to other studies, where the shape of the enhanced component matches the persistent spectrum outside of the burst (see, e.g., Figure 4 of in 't Zand et al. 2013). Further burst observations with *NICER* and additional theory/spectral modeling efforts will be instrumental in finding a more self-consistent physical description of superexpansion bursts.

5. Conclusions and Outlook

We have presented the first strong PRE burst from 4U 1820–30 observed with *NICER*. Because of *NICER*'s soft-band coverage, the properties of the thermal emission could be traced even when the blackbody temperature dropped to 0.45 keV and the radius increased by a factor 30. Furthermore, in the soft band a Comptonization component was detected that accounts for up to 71% of the energy flux. Because the total flux during PRE remained at the Eddington limit, we speculate that part of the neutron star was covered by the accretion environment, and the thermal emission from the neutron star was Comptonized. At the end of the PRE phase, the neutron star was uncovered due to geometrical changes.

The properties of the blackbody match to first order the predictions from models of steady-state outflows. Currently, there exist neither detailed time-dependent models nor models that include the interaction with the accretion environment (e.g., Ballantyne & Everett 2005). Our findings indicate these as important topics for improvement.

In a forthcoming paper we will study the other four bursts from 4U 1820–30. Anticipating improvements in *NICER*'s gain calibration and response model, we will search for discrete spectral features from the neutron star surface and the wind. Moreover, we will investigate constraints on the neutron star's mass and radius that can be derived from the PRE phase. Further *NICER* observations of 4U 1820–30 may catch a burst at lower persistent flux, where the mass accretion inflow is smaller than the wind outflow, leading to different expansion behavior and the possibility of detecting redshifted absorption features (in 't Zand et al. 2012).

ORCID iDs

D. Chakrabarty ⬤ https://orcid.org/0000-0001-8804-8946
J. Chenevez ⬤ https://orcid.org/0000-0002-4397-8370
T. Güver ⬤ https://orcid.org/0000-0002-3531-9842
J. Homan ⬤ https://orcid.org/0000-0001-8371-2713
G. K. Jaisawal ⬤ https://orcid.org/0000-0002-6789-2723
S. Mahmoodifar ⬤ https://orcid.org/0000-0003-2386-1359
C. B. Markwardt ⬤ https://orcid.org/0000-0001-9803-3879

References

Arnaud, K. A. 1996, in ASP Conf. Ser. 101, Astronomical Data Analysis Software and Systems V, ed. G. H. Jacoby & J. Barnes, 17
Ballantyne, D. R., & Everett, J. E. 2005, ApJ, 626, 364
Ballantyne, D. R., & Strohmayer, T. E. 2004, ApJL, 602, L105
Costantini, E., Pinto, C., Kaastra, J. S., et al. 2012, A&A, 539, A32
Cumming, A. 2003, ApJ, 595, 1077
Ebisuzaki, T., Hanawa, T., & Sugimoto, D. 1983, PASJ, 35, 17
Galloway, D. K., & Keek, L. 2017, arXiv:1712.06227
Galloway, D. K., Muno, M. P., Hartman, J. M., Psaltis, D., & Chakrabarty, D. 2008, ApJS, 179, 360
Gendreau, K., & Arzoumanian, Z. 2017, NatAs, 1, 895
Gendreau, K. C., Arzoumanian, Z., Adkins, P. W., et al. 2016, Proc. SPIE, 9905, 99051H
Grindlay, J., Gursky, H., Schnopper, H., et al. 1976, ApJL, 205, L127
Grindlay, J. E., Marshall, H. L., Hertz, P., et al. 1980, ApJL, 240, L121
Güver, T., Wroblewski, P., Camarota, L., & Özel, F. 2010, ApJ, 719, 1807
He, C.-C., & Keek, L. 2016, ApJ, 819, 47
in 't Zand, J. J. M., Cumming, A., Triemstra, T. L., Mateijsen, R. A. D. A., & Bagnoli, T. 2014, A&A, 562, A16
in 't Zand, J. J. M., Galloway, D. K., Marshall, H. L., et al. 2013, A&A, 553, A83
in 't Zand, J. J. M., Homan, J., Keek, L., & Palmer, D. M. 2012, A&A, 547, A47
in 't Zand, J. J. M., Visser, M. E. B., Galloway, D. K., et al. 2017, A&A, 606, A130
in 't Zand, J. J. M., & Weinberg, N. N. 2010, A&A, 520, A81
Jahoda, K., Markwardt, C. B., Radeva, Y., et al. 2006, ApJS, 163, 401
Joss, P. C., & Melia, F. 1987, ApJ, 312, 700
Kajava, J. J. E., Koljonen, K. I. I., Nättilä, J., Suleimanov, V., & Poutanen, J. 2017, MNRAS, 472, 78
Keek, L., Arzoumanian, Z., Bult, P., et al. 2018, ApJL, 855, L4
Kuulkers, E., den Hartog, P. R., in 't Zand, J. J. M., et al. 2003, A&A, 399, 663
Nobili, L., Turolla, R., & Lapidus, I. 1994, ApJ, 433, 276
Paczynski, B. 1983, ApJ, 267, 315
Paczynski, B., & Proszynski, M. 1986, ApJ, 302, 519
Prigozhin, G., Gendreau, K., Foster, R., et al. 2012, Proc. SPIE, 8453, 845318
Revnivtsev, M. G., Suleimanov, V. F., & Poutanen, J. 2013, MNRAS, 434, 2355
Stella, L., Priedhorsky, W., & White, N. E. 1987, ApJL, 312, L17
Suleimanov, V., & Poutanen, J. 2006, MNRAS, 369, 2036
Suleimanov, V., Poutanen, J., & Werner, K. 2012, A&A, 545, A120
Titarchuk, L. 1994a, ApJ, 434, 570
Titarchuk, L. 1994b, ApJ, 429, 340
Valenti, E., Ferraro, F. R., & Origlia, L. 2004, MNRAS, 351, 1204
van Paradijs, J., & Lewin, W. H. G. 1987, A&A, 172, L20
Weinberg, N. N., Bildsten, L., & Schatz, H. 2006, ApJ, 639, 1018
Wilms, J., Allen, A., & McCray, R. 2000, ApJ, 542, 914
Worpel, H., Galloway, D. K., & Price, D. J. 2013, ApJ, 772, 94
Zhang, G., Méndez, M., Belloni, T. M., & Homan, J. 2013, MNRAS, 436, 2276